Journal of Al-Azhar University Engineering Sector

Vol. 20, No. 74, January 2024, 255 - 275

THE EFFECT OF INFLOW TURBULENCE ON THE PERFORMANCE OF SMALL-SCALE WIND TURBINE

Mohamed Fakhr [1] *, Mohamed Emam [1, 2], M. Moawed [1], M.A. Abdelrahman [1]

[1] Combustion and Energy Technology Lab, Mechanical Engineering Department, Shoubra Faculty of Engineering, Benha University, Egypt

[2] Department of Energy Resources Engineering, Egypt-Japan University of Science and Technology (E-JUST), Alexandria 21934, Egypt.

***Correspondence:** mohamed.fakhr@feng.bu.edu.eg

Citation:

M. Fakhr, M. Emam, M. Moawed and M. A. Abdelrahman " The Effect Of Inflow Turbulence On The Performance Of Small-Scale Wind Turbine", Journal of Al-Azhar University Engineering Sector, vol. 20, pp. 255 - 275, 20٢5.

Received: 05 Novmber 2023

Revised: 27 December 2023

Accepted: 25 January 2024

Doi: 10.21608/auej.2025.245905.1457

ABSTRACT

The current study explores the impact of inflow turbulence on the aerodynamic performance of a small-scale wind turbine With respect to power coefficient and wake recovery location on various terrains representing different topographical locations. A comprehensive 3D model is developed and validated to simulate the small-scale horizontal axis wind turbine's aerodynamic performance operating in an atmospheric boundary layer caused by surfaces with various aerodynamic roughness lengths. The k-ω SST turbulence model is utilized to solve transient Reynolds averaged Navier-Stokes equations, revealing critical wake characteristics as wake velocity and turbulence intensity recovery. wake velocity behind wind turbines is accelerated by increasing inflow turbulence. According to the study, for the no atmospheric boundary layer case wake velocity recovered after over twenty times the turbine diameter. Changing tip speed ratio has minimal impact on the power coefficient, except for a marginal 6 percent improvement at the 3 and 7.1 ends. By evaluating the viability of putting turbines behind the front row for the best power coefficient and lowest operating and maintenance costs, the research seeks to improve wind farm efficiency.

KEYWORDS: Free stream turbulence, wind farm, wind turbine Wakes, Atmospheric boundary layer, CFD simulations.

تأثير اضطراب التدفق على الأداء الديناميكي الهوائي لتوربينات الرياح صغيرة الحجم

محمد فخر[١] *، محمد امام[١ ٢] ، محمد معوض[١]، محمد عبد الرحمن[١]

[١] قسم الهندسة الميكانيكية ، كلية الهندسة بشبرا ، جامعة بنها ، معمل تكنولوجيا الطاقة والاحتراق ، القاهرة ، مصر

[٢] قسم هندسة الطاقة والموارد ، الجامعة المصرية اليابنية للعلوم والتكنولوجيا, الاسكندرية ٢١٩٣٤ ، مصر

*البريد الالكترونى للباحث الرئيسي : Mohamed.fakhr@feng.bu.edu.eg

الملخص

تستكشف الدراسة الحالية تأثير الهواء المضطرب في الدخول على اداء توربينات الرياح صغيرة الحجم من حيث معامل القدرة وموقع اختفاء اثر التوربينة على أنواع مختلفة من التضاريس والتى تمثل مواقع جغرافية مختلفة. تم تطوير نموذج ثلاثي الأبعاد شامل والتحقق من صحته لمحاكاة الأداء الديناميكي الهوائي لتوربينات الرياح صغيرة الحجم ذات المحور الأفقي والتي تعمل في الطبقة الحدودية الجوية الناجمة عن أسطح لها أطوال خشونة هوائية مختلفة. يستخدم النموذج نموذج الاضطراب k-ω SST لحل معادلات رينولدز المتوسطة نافيير ستوكس غير المستقرة للكشف عن خصائص الاثر المهمه مثل سرعة الهواء واستعادة شدة الاضطراب. تكشف الدراسة أن ارتفاع اضطراب التدفق

يؤدي إلى تسريع تعافى سرعة الهواء خلف توربينات الرياح، حيث تتعافى في حالة الأسطح الملساء بعد أكثر من عشرين ضعف قطر التوربين. تهدف الدراسة إلى تحديد مدى جدوى وضع التوربينات خلف الصف الأمامي للحصول على معامل طاقة أمثل وتكاليف تشغيل وصيانة منخفضة.

الكلمات المفتاحية : اضطراب التيار الحر، الطبقة الحدودية للغلاف الجوي، مزرعة الرياح، اثر توربينات الرياح، محاكاة CFD

1. INTRODUCTION

The atmospheric boundary layer (ABL), various wind shear, turbulence intensity (TI), and wind speed represents challenges for wind turbine design. The terrain roughness, wind direction, and the ABL stability all influence ABL features, which is also controlled by the atmosphere vertical temperature distribution which can be characterised by its ability to withstand vertical motion or suppress already-existing turbulence into stable, neutrally stable, and unstable stratification. Whereas stable stratification happens when rising air becomes colder than its surroundings, inhibiting vertical air movement, unstable stratification happens when surface heating drives warm air to rise, creating convection cell and thick boundary layer. In neutral environments, air rises in thermal balance with its surroundings.[1]. These flow characteristics have been showed to significantly impact the wake flow structure of wind turbines.[2 – 4]. particularly two major variables that have acquired a lot of attention in wind turbine research. First, the wake velocity deficit which leads the downstream wind turbines to gather less power, hence lowering the total efficiency of the wind farm. Second, the increased turbulence in the wakes which may cause higher fatigue loads and a shorter service life for downstream wind turbines [3].

The Horns-Rev offshore wind farm serves as an example of how ABL inflow turbulence significantly affects both the wake recovery as well as the wind farm's total power production, Hansen et al [5] discovered that when the incoming flow's TI increased from 3 percent to 12 percent, the gathered power from turbines in the second row operating in the wakes of turbines in the first row increased from 0.5 to 0.7 of the first row turbines' power. Hence Comprehending the aerodynamic properties of the turbine wake in various incoming ABL flow circumstances is imperative for optimising wind farm design, specifically turbine placement, in order to augment power generation and reduce maintenance expenses.

wind turbine wake formes owing to the differential pressure between the blades' suction and pressure sides when wind interacts with the blades causing tip vortices to form, these vortices at the tips of each blade revolve against the direction of the rotor, following a helical path downstream. Tip vortices on helical trajectories form a cylindrical shear layer as they are near to each other. because of their tiny tilt angle [2]. This layer segregates the low velocity wake from the ABL flow. Because of turbulent mixing or diffusion The shear layer widens as it moves downstream. [2]. Ambient turbulence enhances turbulence mixing and expedites wake recovery. [6]. The ABL 2D advancement downstream the turbine is illustrated in **Fig. 1a**. As we proceed downstream, the mean speed will gradually recover and the velocity deficit gets flatten.

(b) (c)

Fig. 1. (a) concept representation of wind turbine wake operating in an ABL (b) conceptual and actual ABL (c) conceptual and actual wake profile [4].

The separation layer reaches the centre of wake at a certain distance downwind. The zone up to this point is described as the zone of near wake [2] wherein the blades number and the blades' aerodynamics can be sensed [2]. By this definition, as the shed vortices are directly linked to the radial fluctuation of the bound vorticity over the blades and the helical vortex system created within the rotor's back remains stable and recognisable. Thus, the near wake zone may extend several diameters downstream the rotor, contingent upon the rotor loads and the inflow circumstances [7] .

the near wake zone is followed by the far wake zone wherein the wake dynamics are unaffected by rotor features. Here, the rotor-generated vortex system is totally destroyed, and small-scale turbulence controls the field of flow [6].

Wind turbine wakes have been discussed in many experimental and numerical papers, Chamorro et al. [8] investigated the turbulence that originated behind a little wind turbine situated within the boundary layerthat evolved over both smooth and rough surfaces using wind tunnel experimentation on a 0.15 m diameter 3 blades horizontal axis wind turbine (HAWT), which were created by placing 5mm-height chains in tunnel test section, aligned perpendicular to flow direction, under neutral stability conditions. Unlike axisymmetric wakes created in homogeneous free stream flows, the inflow inhomogeneity creates The turbulence's asymmetry which increases with increasing surface roughness owing to the irregular formation of TI and velocity at the intake. Also Gambuzza et al. [9] and Li et al. [10] utilized the active grid technique to generate turbulence and found that the power coefficient is highly reliant upon the infow TI. Additionally, the flow separation on the blade's suction side is affected by turbulence. The degree of TI in the inflow had a noteworthy effect on the efficiency and recovery of wakes of the array's two turbines.

Talavera et al. [11] examined in an experimental setting both an array with two turbines and a freestanding 0.203 m diameter two-blade HAWT model in both laminar and turbulent flow conditions using active-grid to generate the free stream turbulence, unlike prior research that employed the active-grid to generate mechanical turbulence, which is different from ABL turbulence, turbulent flow was created utilising an active grid system with the gid motor rotation adjusted to approximate ABL profile at the intake.

As stated by the previous literature on the experimental research the inflow turbulence impacts wind turbine performance, the majority of the previously studied papers in wind tunnels faces limitations such as variable size, blocking, and scaling effects as is evident from all studied cases, the turbine diameter is maximum 0.2 m, which may not be relevant to large-scale turbines. Also, the lack of monitoring stations and uncertain flow characteristics for field measurements hardens evaluating the wakes downstream the turbine.

Owing to the difficulties explained in experimental work, numerical investigations have gained a lot of attention. To simulate the ABL, the vertical wind profiles should be correctly measured using anemometer-equipped masts to measure the speed of the wind throughout time. It is cost effective and time saving to utilise mathematical equations that predict the wind shear vertical profile. The wind speed vertical profile over flat homogenous terrain can be theoretically modelled using two popular mathematical models to simulate the ABL velocity profile: power and log laws [12]. The theoretical and realistic velocity profiles do not match up, as **Fig. 1b** and **1c** show, because early theoretical forecasts ignored the consideration of dynamics of 3-dimensional air turbulent stream connected to near field and local topography. Furthermore, as theoretical profiles are one-dimensional horizontal shear wind simulations [4]. Generally, the theoretical models of the vertical velocity profile are discovered to be cost effective and time saving method in simulating wind turbine ABL.

There are two primary types of wake models.: explicit and implicit types. First explicit models use a self-similar velocity profile and are often employed in industry owing to their accuracy and efficiency. Field models, which solve Parabolized Navier-Stokes equations, are more computationally expensive but produce better projections. Elliptic field/full CFD models solve Navier-Stokes equations with the turbines as a sink component, using either actuator-disc (AD) technique or actuator-line (AL) approach. These models require parameter tweaking and adequate wake initialization.

Wu et al. [13] used an AD approach and large eddy simulation (LES) to conduct a numerical research to examine the influence of various ABL roughness lengths on Vestas V80-2MW stand-alone HAWT wake assuming neutral stability. Also, Panjwani et al. [14] studied the effect of marine ABL on wind farms using AD approach on the same model. The primary drawback of the AD approach is that, because the forces at each spanwise section are uniformly distributed in the azimuthal direction, it is limited to rotationally symmetric flow circumstances. Additionally, it proposes that the blades are viewed as an integral component of the circumferential direction, hence, the method is unable to consider the tip vortices impact. Troldborg, N. [7] investigated, using an AL-based model and LES, the Tjæreborg turbine's wake while it was operating in a turbulent inflow with a standard mean shear. Comparable to what was observed in the laminar inflow scenario, wake rotation was also demonstrated to cause the wake to become horizontally asymmetric. But the imbalance seemed to progressively disappear as wake split up and grew more erratic. Kabir et al. [15] conducted a study on a full rotor HAWT NREL Phase VI using unsteady k-ε turbulence model. Results showed that increased wind shear due to roughness length recovers faster. However, the k-ε turbulence model overpredicted rotor aerodynamics, requiring a better model for near wall cell flow prediction.

It is clear from evaluating earlier research on the aerodynamics of wind turbine operating in ABL that inflow turbulence significantly affects turbine performance.

Small-scale HAWT may be installed on different topographic sites to harness wind energy for the production of electricity. Unlike big HAWT, which are situated in the buffer or turbulence zone as depicted in **Fig. 1b**, turbines working in these zones will operate in the ABL's viscus sublayers, that have a nonuniform velocity profile. In light of this, the current study investigates how inflow turbulence affects a small-scale wind turbine's wake recovery position and power coefficient at different TSR positioned at different terrain types. The present paper used the log law to define four mean vertical velocity profiles for varying roughness lengths. The NREL S826 airfoil was utilised to create a three-blade, small-scale HAWT with a rotor diameter of 0.9 m. The model was drawn to simulate the full rotor performance operating in ABL that is developed by surfaces with different aerodynamic roughness lengths that correspond to different topographies. The novality of the paper is to extend the k ε standard model proposed by Richards [16] to the unsteady k-ω SST turbulence model due to its ability to capture the near wall analysis [15] to simulate small scale wind turbines operating in different ABL conditions.

2. Physical Model description.

Fig. 2 displays the full dimensions of the physical model and boundary conditions utilized in this study. The computational domain is a 0.9 m-diameter wind turbine rotor with three blades; the blades are based on the NREL S826 airfoil, and Krogstad et al. provided the rotor design parameters, such as chord and twist variation over the span [17]. Next, to replicate the spinning of the rotor, a cylindrical domain enclosing it is filled with meshing elements that revolve as per the TSR being tested. The turbine rotation is accomplished by using sliding mesh, which is good at forecasting rotational flows and can accurately characterize the entire transient setup. Furthermore, unlike the AD and AL techniques, the rotor is simulated using a fully drawn geometrical model, which is thought to produce better results. However, this technique requires a lot of computational resources and may not be suitable for large wind farm simulations. The cylindrical rotating domain, which represents the air surrounding the turbine, is bounded by a stationary box known as the main domain. The main domain extends 20D downstream and 2D upstream the rotor, where D is the rotor diameter. This short distance upstream the rotor is necessary to prevent mandated inflow

turbulence decline. The wind turbine is surrounded by a spinning cylindrical domain, as presented in **Fig. 2**, and its main domain height is 10D. the hub height has been chosen to be equal to 5D to simulate the small-scale wind turbine operating conditions which can be mounted on small towers ranges from 4 to 6 meters while the top boundary at 10D from the ground to keep the rotor swept area below 10% of the tunnel cross section for the measured drag forces not to be seriously affected by wall interference [18] and to facilitate domain discretization on a symmetric structured mesh which saves computational time and memory.

Fig. 2. The computational domain used in the current study with dimensions and boundary conditions.

By virtually situating the model wind turbine over the bottom wall or ground with changing roughness lengths, the impact of different ABLs on wind turbine wake characteristics were examined. The representative terrain types and the roughness lengths that were used are shown in **Table 1.**

Table 1: Typical surface roughness lengths [1].

Types of landscapes	**Roughness Length z_o (m)**
smooth desert, choppy sea	0.001
grassy, level plains	0.01
villages and a rural area with hedges and trees	0.1
Cities and woods	0.7

3. GOVERNING EQUATIONS

This study aims to investigate the impact of ABL on the power coefficient and wake features of wind turbines. The homogeneous ABL must be precisely modelled in the CFD study for reliable findings. The turbulent characteristics of the ABL applied at the inlet and the vertical velocity profile in the computational domain deteriorate with downstream distance due to the ground roughness features and fully developed ABL failing to remain in balance. to preserve the velocity profile horizontal homogeneity and the turbulence quatities up to the turbine position, it is imperative to accurately model the ground roughness characteristics [16], [19].

3.1 Bottom (ground) boundary condition

Every CFD simulation of the bottom wall requires a realistic depiction of the flow near the wall. In wall functions in fluent, the sand-grain size kS corresponds the wall roughness zo. To accuratly simulate the bottom wall four conditions must be met simultaneously. [16], [20], [21]:

1. a vertically appropriate high mesh resolution (e.g., first cell height < 1 m) towards the bottom wall.
2. Both the top and bottom portions of the domain exhibit horizontal homogeneity in ABL flow.
3. The sand grain size (k_S) is not to be more than the distance (y_P), which is defined as the distance between the neighbouring cell centre point and the bottom wall.
4. Equation (1) defines the relation between roughness length (z_o) and k_S in Fluent.

$$k_s = \frac{9.793 \times z_o}{C_s} \qquad \text{Eq. (1)}$$

where the default value of ANSYS FLUENT is 0.5 and the roughness constant is Cs.

The height of the cells near the bottom wall shall be at least twice kS height when taking the third condition into account. The zo values utilized in this work are those found in Table 1 and to meet the fourth criteria for zo = 0.7 m as stated in Eq. 1. The associated kS value for Cs = 0.5 (the default value) will be 13.7 m, corresponding to a cell height of 2 × 13.7 m that is higher than

the height of the entire domain. Furthermore, the first condition states that the first cell's height must be less than one metre. Or otherwise, Labovský et al.[22] suggested raising the Cs values to keep kS value at the right level to meet the FLUENT requirements. In FLUENT Graphical User Interface (GUI) Cs value can be varied between 0 and 1 which will result in high value of Ks that will contradict with the above requirements, so a compiled User Defined Function (UDF) was used to assign the appropriate value of Cs.

3.2 Fully developed ABL profile

Richards et al. [16] suggested using the wind speed logarithmic vertical velocity profile (Eq. 2), assuming fully developped neutral ABL, using k-ε turbulence model, kinetic energy of turbulence (Eq. 3) and rate of turbulence dissipation (Eq. 4). One crucial premise is that the shear stress will remain constant with the ABL height [16], [21], [23].

logarithmic mean wind velocity U(z):

$$U(z) = \frac{U_{ABL}}{K} \ln\left(\frac{Z + Z_o}{Z_o}\right) \quad \text{Eq. (2)}$$

Turbulence Kinetic energy (k):

$$k(z) = \frac{U_{ABL}^{*\,2}}{\sqrt{C_\mu}} \quad \text{Eq. (3)}$$

Turbulence dissipation rate (ε) :

$$\varepsilon(z) = \frac{U_{ABL}^{*\,3}}{K.(Z_o + Z)} \quad \text{Eq. (4)}$$

where, z_o is the roughness length of th terrain (m), z is the height above the lvevl of th ground (m), K is the von-Karman constant = 0.4, and $C\mu$ is the k-ε turbulence model constant.

Since the near wall analysis does not work well with the Standard k-ε model [24]. Yang et al. and Per Blocken et al.[21], [25] The turbulence kinetic energy and turbulence dissipation rate profiles can be converted to the appropriate profiles using these equations, which can also be extended for additional turbulence models. Given that the k ω (SST) model can accurately forecast the near wall analysis and because of that the k ω (SST) model has been chosen. Yang et al [26] suggested to alter the ε profile to one for the specific dissipation rate ω, which is defined as:

$$\omega = \frac{U_{ABL}^{*}}{K\,x\sqrt{C_\mu}} \frac{1}{(Z + Z_o)} \quad \text{Eq. (5)}$$

To define the inlet boundary condition Eq.2, Eq.3 and Eq.5 were applied. An outflow boundary condition was applied to the output, presuming that the flow is fully developed and that streamwise or normal gradients equal zero. [15], [21] . regarding two lateral edges The symmetry condition i.e zero gradient was used. [15]. At the top surface, a continuous shear stress shall be utilized to preserve horizontal homogeneity. [16], [21] It is possible to achieve by treating the top surface as a velocity inlet in the flow direction [21], [23]. The walls of the rotor were subjected to a no slip condition.

3.3 TI profile in the wake

The TI is defined as the ratio of standard deviation of the fluctuation wind velocity to the mean wind velocity [1].

$$TI = \frac{\sigma_u}{\bar{u}(z)} \quad \text{Eq. (6)}$$

The link between k and TI is given by Eq. 7 [27], [28]. It is more practical to use this equation, particularly when determining the TI after the CFD analysis is finished.

$$TI = \frac{\sqrt{\frac{2k}{3}}}{\bar{u}(z)} \quad \text{Eq. (7)}$$

Eq. (8) can be used to express the total TI in the wake.

$$TI_{wake} = (\,TI_{+}^{2} + TI_{a}^{2}\,)^{1/2} \quad \text{Eq. (8)}$$

3.4 Turbine power coefficient

A popular measure of wind turbine efficiency is the power coefficient, which is computed by dividing the actual power gathered by the turbine to the total available incoming wind power at a specific wind speed.

$$C_p = \frac{T\,\omega}{0.5\rho A u_{hub}^3} \quad \text{Eq. (9)}$$

where U_{hub} is the freestream velocity at hub height and C_P is the power coefficient . The power coefficient is determined by measuring the freestream velocity at height of the hub, which roughly corresponds to the average turbine design alone. Nevertheless, the inflow velocity is faster at the higher blade and slower at the lower blade.

4. Numerical methodology and Mesh independence study

The meshing of the model was performed using ANSYS mesher. The inner small-scale rotating domain consists of about 10.42 M tetrahedral element as shown in **Fig 3** and an inflation with a first layer thickness of 10-5 meter were created around the blades to ensure y plus less than unity to capture the local skin-friction on a smooth flat plate for turbulent boundary layer as shown in **Fig. 3b** and **c** [20], respectively, while the main domain consists of 0.92 M hexahedral elements as shown in **Fig. 3a** the main domain was divided into 3 zones on upwind, one downwind and at rotor plan to convert domain into mappable volumes that can be meshed using hexahedral mesh as shown in **Fig. 3a**. To ensure that the mesh density has no effect on the results in addition to save the computational time, a grid independence study was done at TSR 5.1 for the no ABL case as shown in **Table 2**.

Table 2: The effect of mesh density on generated aerodynamic torque at TSR 5.1 at no ABL.

Number of elements	Torque (N.M)	Deviation (%)
7.5 M	1.3391	-
9 M	1.4134	5.2
11.34 M	1.4496	2.6
13 M	1.4703	1.4

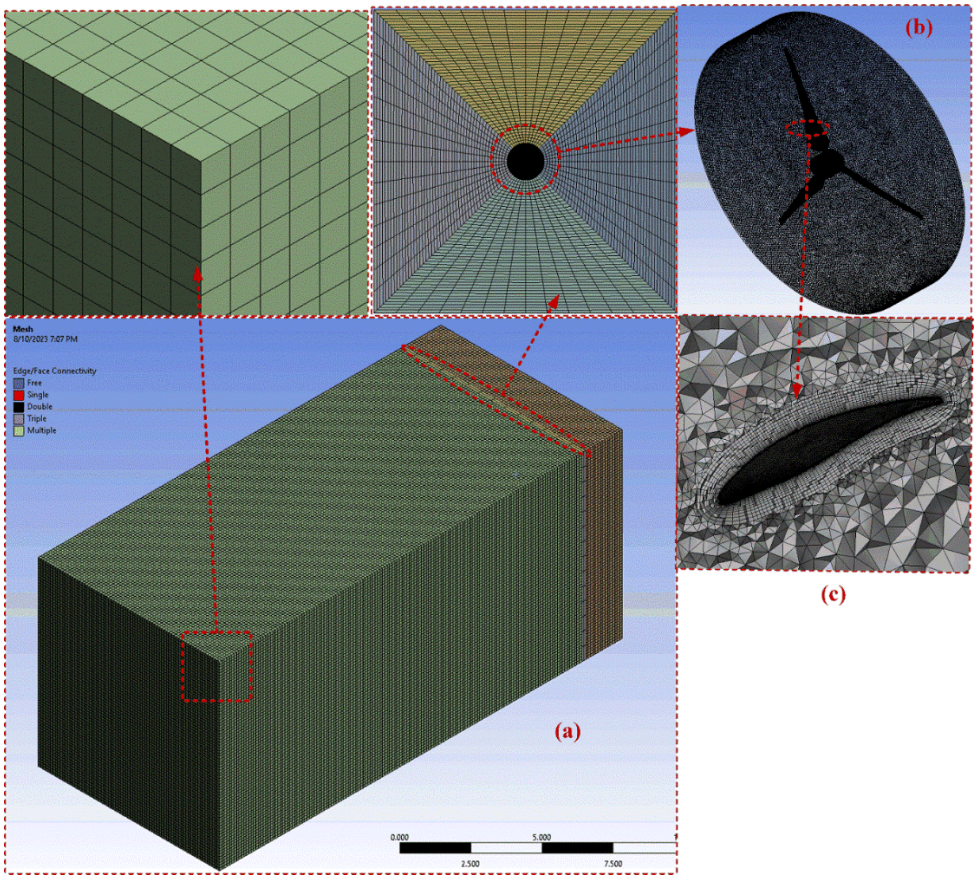

Fig. 3. 3D visualization of the Mesh (a) main domain hexahedral mesh, (b) the cylindrical rotating domain and (c) airfoil inflation layer.

4.1 INFLOW BOUNDARY CONDITION

Using varying topographies, the study investigated the aerodynamic performance of small-scale HAWT working in homogeneous, neutrally stratified ABLs. The study used various roughness lengths, including z_o = 0.7 m, 0.1 m, 0.01 m, and 0.001 m, with a reference velocity of 10 m/s. Because of the increasing wind shear between viscous ABL layers, the results showed that velocity near the ground dropped as surface roughness increased. Blades above the height of the hub encountered wind speeds faster on rough surfaces. The inflow TI profile varies with roughness length, with maximum intensity near the ground.

Blades below the height of the hub experienced higher turbulence intensities, resulting in cyclic fatigue loads. This suggests that turbines operating in high roughness length topography will require shorter service life and higher maintenance costs.

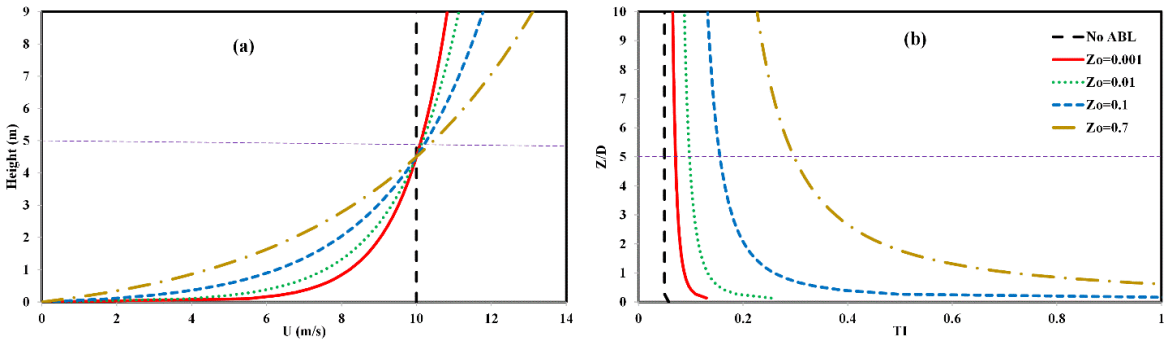

Fig. 4. comparison of (a) vertical inflow velocity profiles and (b) vertical TI profile for four different terrains with different roughness lengths and no ABL profile.

4.2 MODEL VERIFICATION.

The numerical study was validated by prescribing a uniform inflow wind speed of 10 m/s at the "no ABL condition" inlet boundary condition, and plotting the power coefficient against the TSR, which aligns with experimental data by Krogstad et al.[17] as shown in **Fig. 5**.

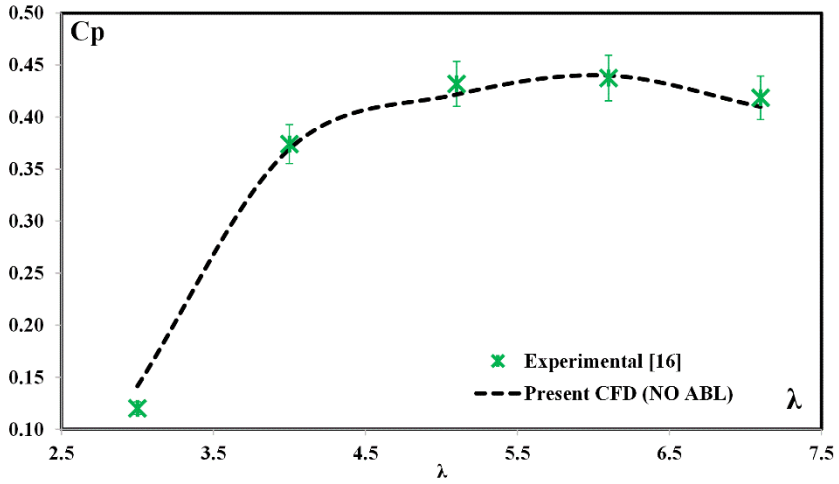

Fig. 5. Power coefficient against TSR for present study (No ABL) against experimental data [17].

5. Results and Discussion

The effect of ABL on small-scale HAWT power coefficient , wake recovery and downstream TI is examined and addressed for different terrain types. Five the inflow velocity profiles used in the study. First case is uniform velocity profile with constant velocity equal to 10 m/s representing No ABL case which was verified with Krogestad [17]. The other four cases used different log law velocity profiles corresponding to different roughness lengths. The results of the power coefficient **Fig 6**, wake velocity profile and velocity contours **Fig. 7,8,9** and **10** and turbulence intensity profile **Fig. 11** are all plotted for the five case to compare the no ABL case with the ABL cases.

5.1 POWER COEFFICIENT.

A smooth surface with a consistent inflow velocity of 10 m/s and a horizontal flat surface with varying ABL profiles were used to plot the power coefficient of a standalone wind turbine. The power coefficient did not significantly alter during the operating range of 4 to 6, which is in line with earlier findings by [15]. The high TI in the ABL, which suppresses periodic pressure oscillations and causes flow instabilities on the suction side of the airfoil, causes a slight modification in the power coefficient with an increase in roughness length for TSR extreme values 3 and 7, where most of the blades operate in the post-stall regime. This increases the airfoil's lift production. Lift is increased and flow separation is slowed in the post-stall regime by high free stream turbulence.[29].

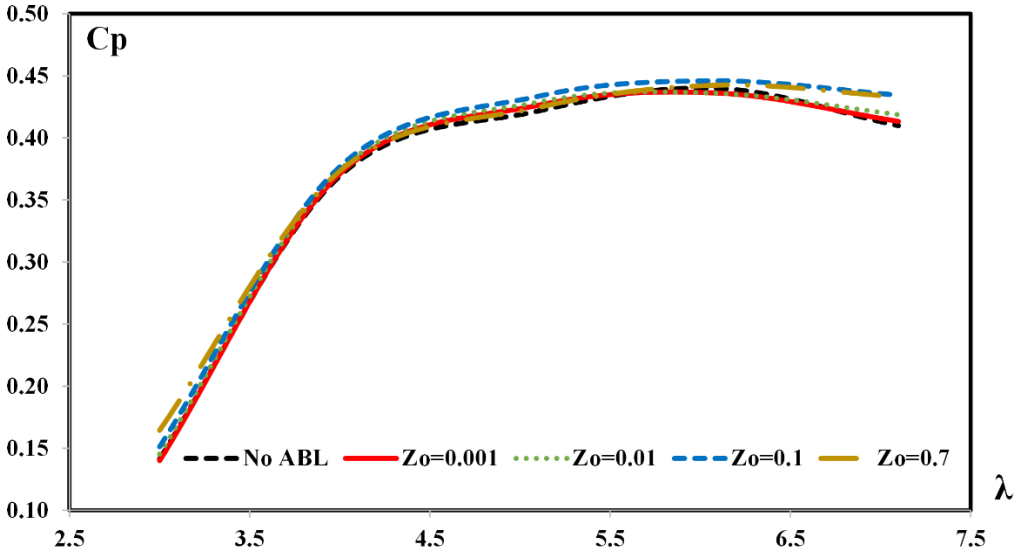

Fig. 6. Power coefficient against TSR for No ABL condition compared to four different terrains with different roughness length.

5.2 WAKE RECOVERY

The wake recovery is studied horizontally and vertically quantitively using velocity profiles and qualitatively using velocity contours to best represent the formation of wake behind the rotor. To generalize the results, the wind velocity is normalized by the velocity at the hub height and the distance behind the turbine is represented in terms of the rotor diameter.

5.2.1 HORIZONTAL PROFILE OF HUB HEIGHT NORMALIZED VELOCITY

Using a step equal to 2D, the study analyses the normalised streamwise velocity profiles and contours at given downstream distances (y/D) between 2 and 20, normalising the wake velocity with the reference velocity and the radial distance in the z direction with the rotor diameter as shown in Fig 7,8. Regardless of the TSR, the wake recovery pattern remains the same. The velocity does not recover to a noteworthy value for the low TI uniform inflow case even at distances higher than 20 D. There is a noticeable degree of divergence in the wake recovery for different wind shears or terrains with different roughness lengths. The more ABL turbulence, the quicker the wake velocity will recover. This is because the ABL turbulence transfers its momentum to the wake, enhancing shear layer turbulent mixing. Although an inlet boundary condition was specified at the top surface of the numerical model, which warped the horizontal normalised velocity profile and contours, a pressure differential between the layers forms at a downstream distance higher than 10D.

5.2.2 VERTICAL PROFILES OF HUB HEIGHT NORMALIZED VELOCITY

Using a step of equal to two times the downstream distance (y/D), the study presented normalised streamwise velocity vertical profiles and velocity contours. It also normalised wake velocity with the reference velocity at height of the hub = 10 m/s and a TSR of 5.1 as shown in Fig 9,10. The findings demonstrated that wind shear in the inflow ABL is the reason for the non-axisymmetric vertical wake profiles in various ABLs. Wake velocity recovers more quickly as the inflow ABL wind shear rises with the lengthening of the rugged terrain.

5.3 TI PROFILE AT DIFFERENT DOWNSTREAM DISTANCES

This study looks into how TI in HAWT is affected by roughness length and height above the ground. As shown in **Fig. 11** TI has an inverse relationship with mean wind speed and a direct relationship with turbulence kinetic energy. If there was no wind shear, the wake's TI at the downstream distance would be symmetric. TI values are influenced by the mean wind speed, which varies with height. The downstream zone's TI profile is subdivided into 2 zones: the near wake ($y/D < 2$) and the far wake ($y/D > 2$), with the former having much higher TI because of strong helicoidal vortex turbulence.

However, because of the turbine's turbulence kinetic energy extraction, the far wake zone encounters a reduction in turbulence strength below the ABL. At all distances, the turbine's placement in the boundary layer causes a non-axisymmetric and non-Gaussian TI distribution. The bottom section's turbine effect is determined by turbulent kinetic energy yield and low mean shear. As the velocity deficit increases, TI in the higher zone falls and eventually returns to the ambient value. The characteristics of the terrain's roughness affect how quickly TI rises. Thus, we deduce that incorrect downstream turbine location that is based solely on velocity recovery may cause the blades to experience incorrect fatigue stresses.

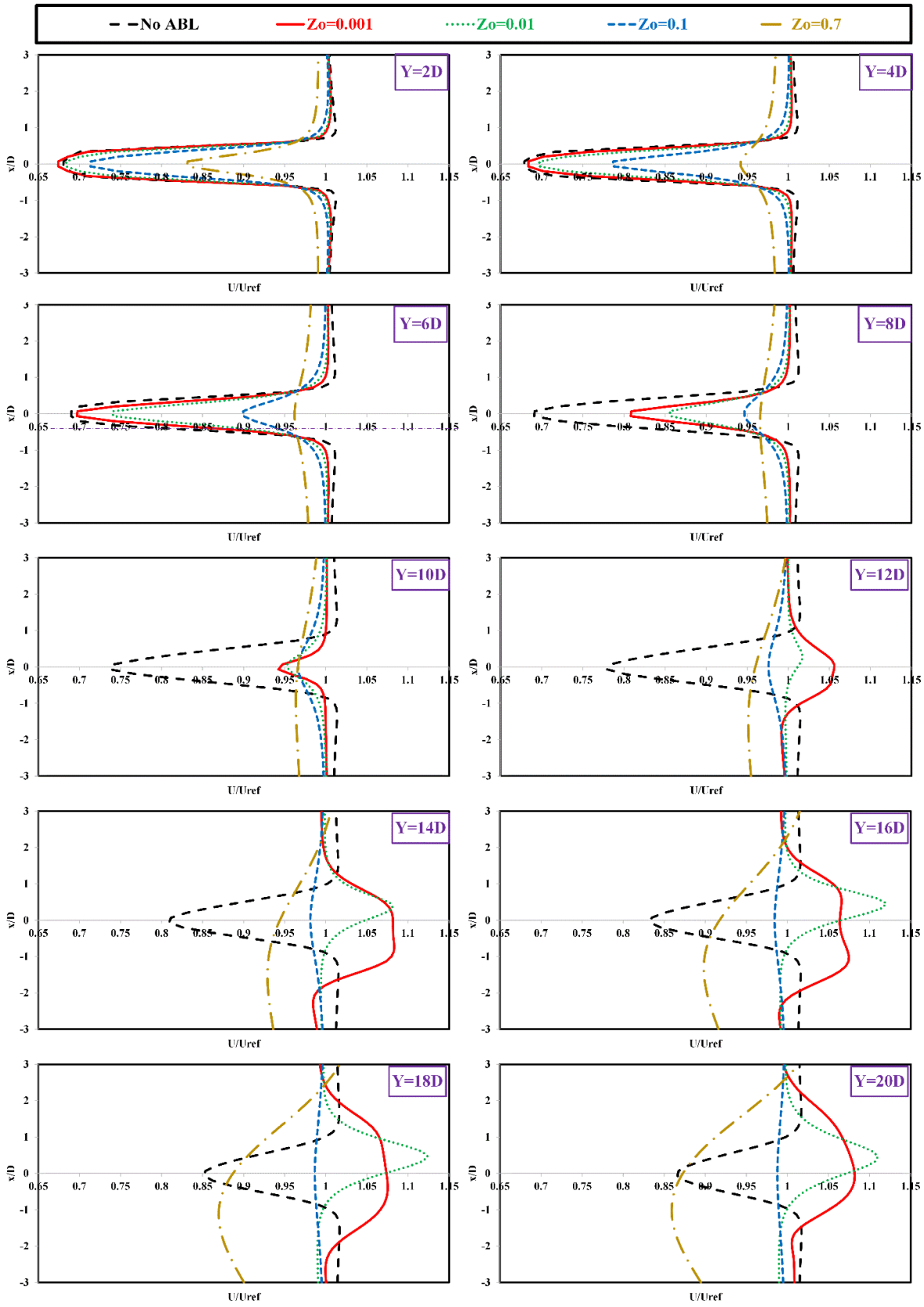

Fig. 7. Horizontal normalized streamwise velocity profiles with different ABL compared to no ABL condition at hub height horizontal sectional plan at different downstream distances Y/D when TSR = 5.1

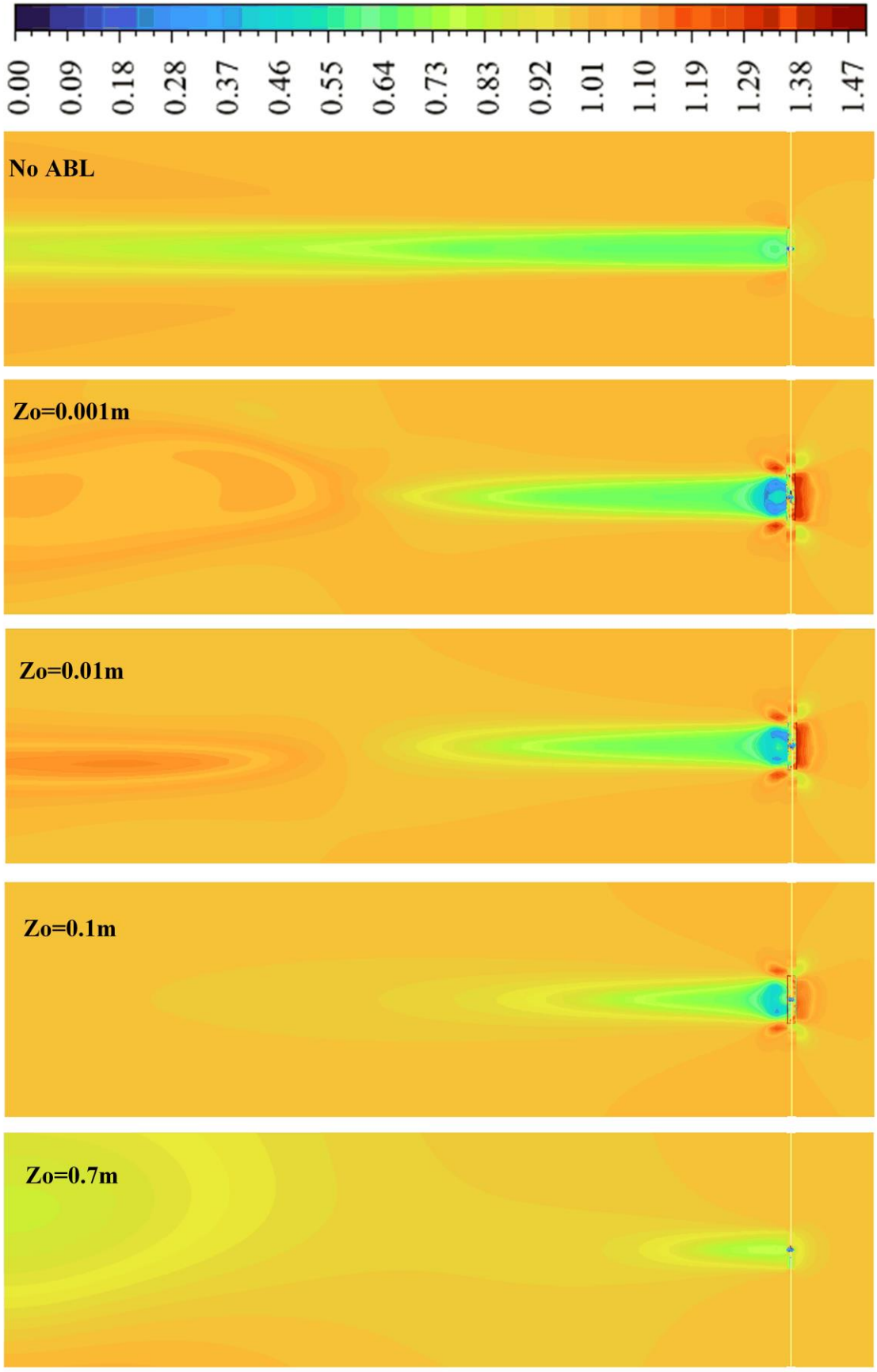

Fig. 8. Horizontal normalized streamwise velocity contours with different ABL compared to no ABL condition at the hub height horizontal sectional plan when $\lambda = 5.1$.

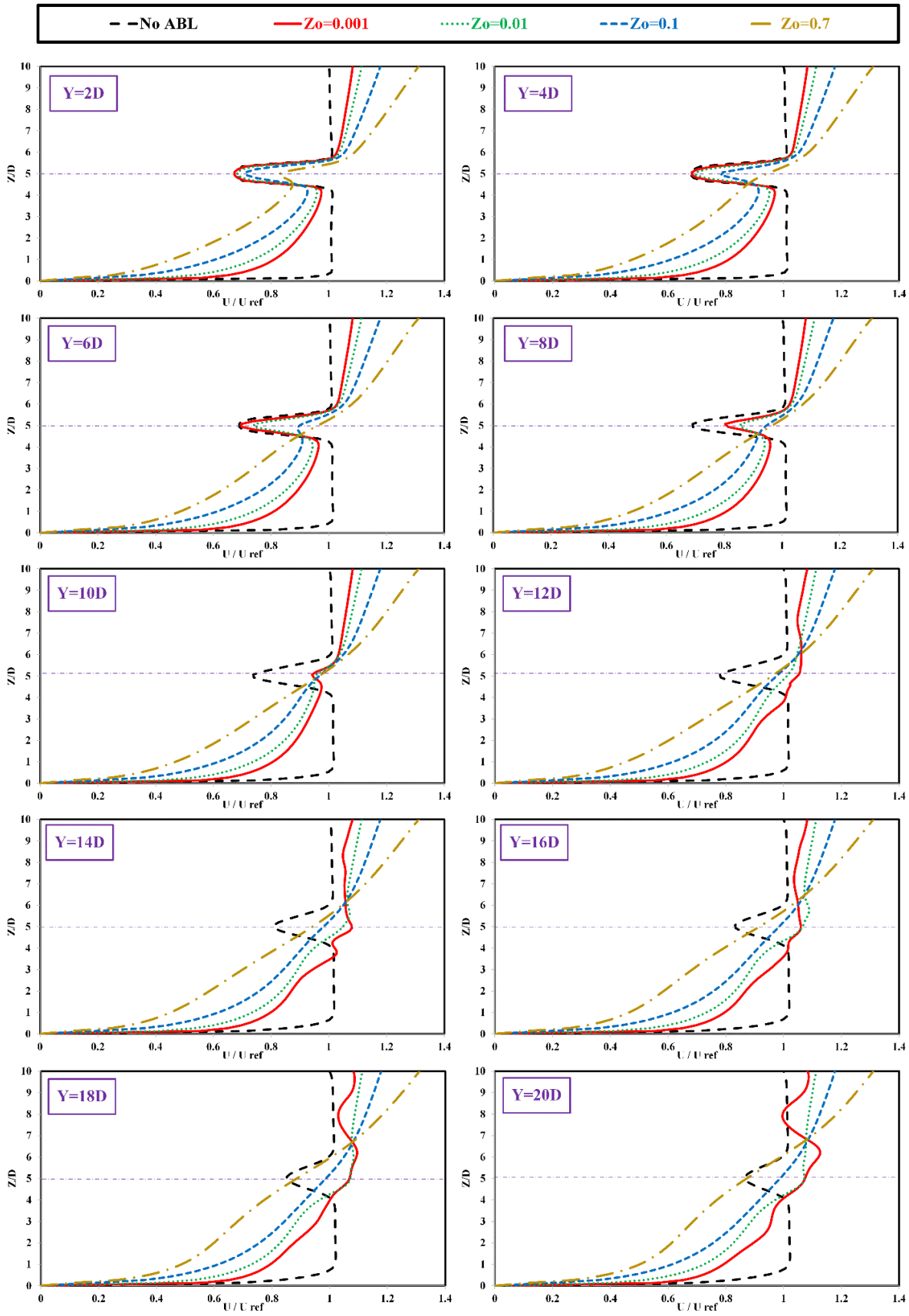

Fig. 9: Vertical normalized streamwise velocity profiles with different ABL compared to no ABL condition at vertical sectional plan at different downstream distances when TSR = 5.1.

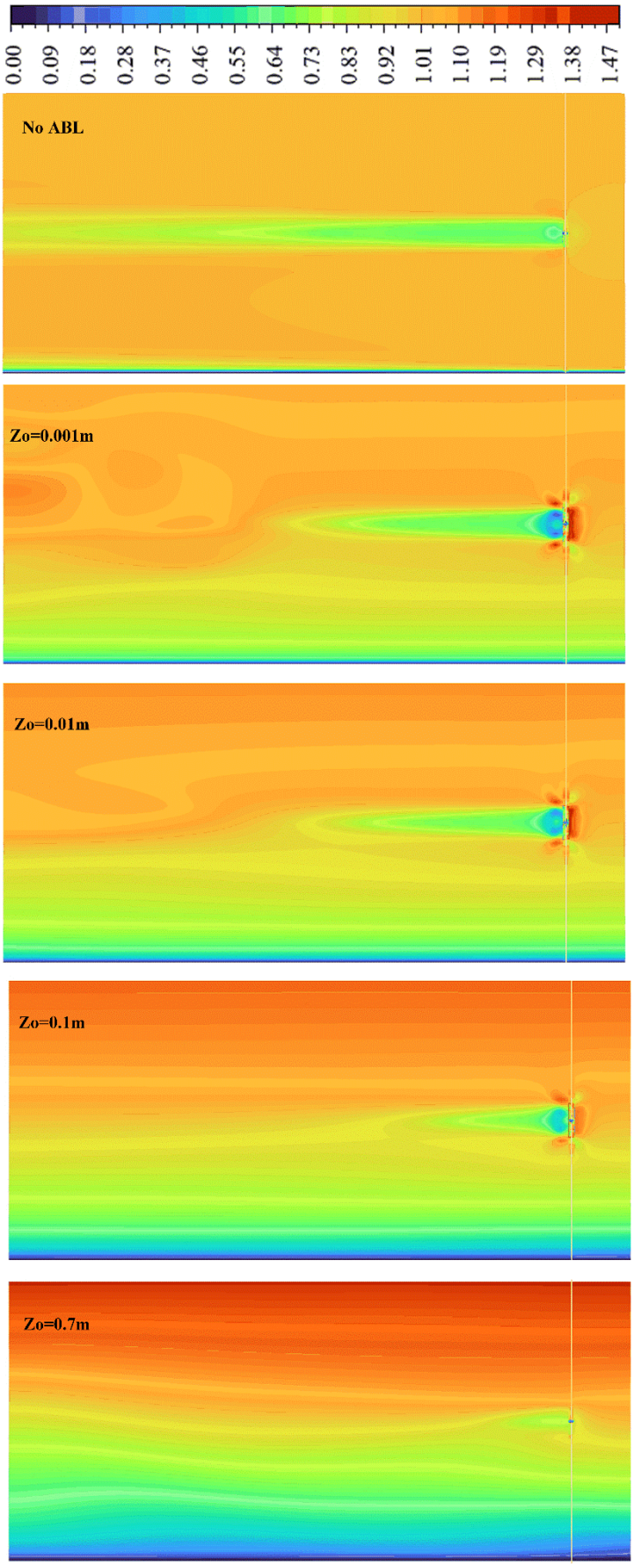

Fig. 10: Vertical normalized streamwise velocity contours with different ABL compared to no ABL condition at the vertical sectional plan when TSR = 5.1.

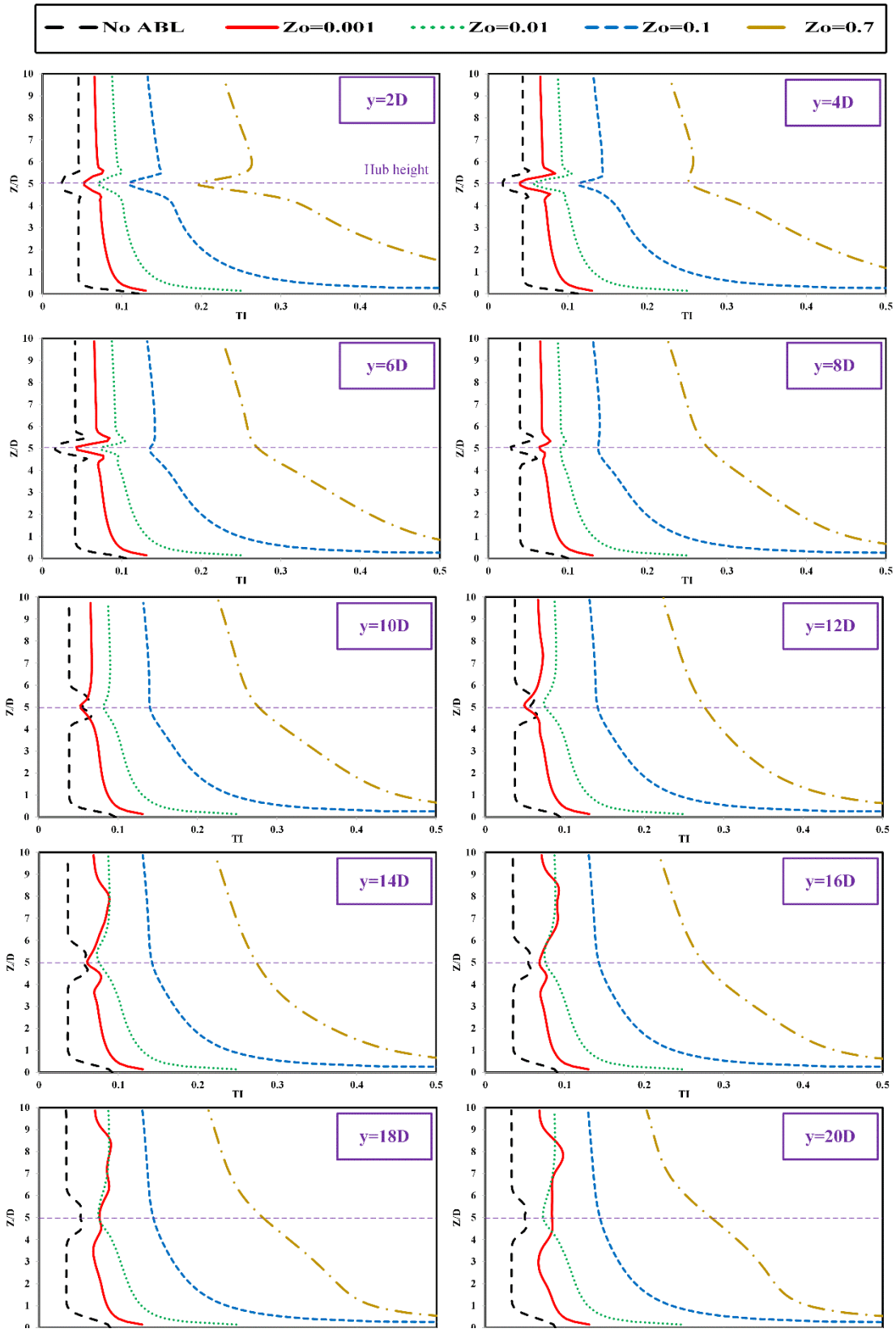

Fig. 11: Vertical TI profiles with different ABL compared to no ABL condition at the height of the hub along the vertical sectional plan at different downstream distances Y/D when TSR = 5.1

6. Conclusion and future work

Numerous numerical analyses were performed to explore the impact of ABL on the power coefficient and the characteristics of small-scale HAWT wake. The URANS simulation was employed to simulate the neutral ABL on flat terrains with different aerodynamic roughness lengths corresponding to different topographic locations. The outcomes demonstrate that the varying wind shears and TI levels of inflow stream caused notable changes in The average velocity deficit's spatial spread and TI in the rotor wake. Revealing that, the turbulent streams across the rugged terrains produced larger turbulent fluxes into the entrained turbine wake and a quicker wake recovery than the smoother streams across the more flat terrain. Changes in the TSR have little impact on the power coefficient , except for a marginal 6 percent improvement at the 3 and 7.1 ends. In all case, the biggest turbulent fluxes and TI levels are observed at the peak of the blade's tip, which is also the position of the greatest mean shear. The maximum TI and fluxes are reached at a distance downstream ranging from 2D to 5D for the roughest and smoothest surfaces respectively. It is demonstrated that the non-axisymmetric wake is less in the smoothest surafce (no ABL). The turbulence added to the wake pertaining to the ABL turbulence level is advantageous above the height of the hub. The altering inflow conditions also led to a significant shift in the amount of the added TI under the height of the hub, where its value turns negative, as the wake of turbine go from smooth to rough surfaces. As recommended by previous studies that the boundary at top should have a fixed shear stress to maintain the horizontal homogeneity, the present study used the inlet boundary condition with the velocity direction parallel to the wind direction. However, after downstream distances greater than 10 D, the vertical normalized velocity profiles show vertical motion due to pressure gradients, which is thought to be the result of the rotor being placed very near to the ground, i.e. in the ABL's viscous sublayer, that is distinguished by a dominant vorticity balance between viscous transport and advective transport of vorticity. The nacelle and tower effects have been excluded from our analysis to simplify the meshing of the model, which is thought to have little impact on the wake and TI profile downstream the wind turbine. However, It might be included in future research for more realistic outputs.

The following topics are recommendations for future work:

- The effect of inflow turbulence on the performance of medium or large-scale wind turbine with their specific operating conditions.
- Long-term effects of varying inflow turbulence on turbine maintenance and wear-and-tear could offer a more comprehensive understanding of performance over time,
- Environmental impacts, such as noise and bird migration interference, alongside an economic analysis like cost-benefit analysis

Nomenclatures

Roman:

k	Turbulence kinetic energy (m^2/s^2)
C_P	Power coefficient (dimensionless)
D	Rotor diameter (m)
k_S	sand-grain roughness (m)
y_P	Dimensionless wall distance
μ	Fluid dynamic viscosity ($N.s/m^2$)
μ_t	turbulent viscosity ($N.s/m^2$)
Γ_k	k effective diffusivity ($N.s/m^2$)
Γ_ω	ω effective diffusivity ($N.s/m^2$)

Abbreviations:

ABL	Atmospheric Boundary Layer
HAWT	Horizontal Axis Wind Turbine

z_o	Roughness length (m)	URANS	Unsteady Reynolds Averaged Navier Stokes
C_s	Dimensionless Roughness constant	SST	Shear Stress Transport
U	Mean wind speed (m/s)	NREL	National Renewable Energy Laboratory
U^*	Friction velocity (m/s)	CFD	Computational Fluid Dynamics
z	Height above the ground (m)	TI	Turbulence Intensity
G_k	generation of k by velocity gradient (kg/(ms^2))	AD	Actuator Disk
G_ω	generation of ω by velocity gradient (kg/(ms^2))	LES	Large-Eddy Simulation
S_k	k user-defined source terms (kg/(ms^2))	AL	Actuator Line
S_ω	ω user-defined source terms (kg/(ms^2))	BEM	Blade Element Momentum
Y_k	dissipation of k due to turbulence (kg/(ms^2))	3D	Three Dimensional
Y_ω	dissipation of ω due to turbulence (kg/(ms^2))	2D	Two Dimensional
D_ω	cross-diffusion term (kg/(ms^2))	GUI	Graphical User Interface
Greek symbols:		UDF	User Defined Function
ε	Turbulence dissipation rate (m^2/s^3)	TSR	Tip Speed Ratio
ω	Specific turbulence dissipation rate s^{-1}		
λ	Tip speed ratio		
ρ	Density (kg/m^3)		

References

[1] N. J. D. S. and E. Bossanyi. Tony Burton, “The Wind Resource,” in Wind Energy Handbook, 2011, pp. 9–38. doi: https://doi.org/10.1002/9781119992714.ch2.

[2] L. J. Vermeer, J. N. Sørensen, and A. Crespo, “Wind turbine wake aerodynamics,” Progress in Aerospace Sciences, vol. 39, no. 6–7. Elsevier Ltd, pp. 467–510, 2003. doi: 10.1016/S0376-0421(03)00078-2.

[3] R. J. Barthelmie et al., “Modelling and measuring flow and wind turbine wakes in large wind farms offshore,” Wind Energy, vol. 12, no. 5, pp. 431–444, 2009, doi: 10.1002/we.348.

[4] Andrew Kay, Dr W K Lee, and Leon Youngs, “Characterisation of Downstream Flow from Large Wind Turbines,” Stanton Avenue Teddington Middlesex TW11 0JZ, 2013.

[5] K. S. Hansen, R. J. Barthelmie, L. E. Jensen, and A. Sommer, “The impact of turbulence intensity and atmospheric stability on power deficits due to wind turbine wakes at Horns Rev wind farm,” in Wind Energy, John Wiley and Sons Ltd, Jan. 2012, pp. 183–196. doi: 10.1002/we.512.

[6] “Aerodynamics of wind turbine wakes Literature review B. Sanderse.”

[7] N. Troldborg, General rights Actuator Line Modeling of Wind Turbine Wakes.

[8] L. P. Chamorro and F. Porté-Agel, “A wind-tunnel investigation of wind-turbine wakes: Boundary-Layer turbulence effects,” Boundary Layer Meteorol, vol. 132, no. 1, pp. 129–149, 2009, doi: 10.1007/s10546-009-9380-8.

[9] S. Gambuzza and B. Ganapathisubramani, “The effects of free-stream turbulence on the performance of a model wind turbine,” Journal of Renewable and Sustainable Energy, vol. 13, no. 2, Mar. 2021, doi: 10.1063/5.0039168.

[10] Q. Li, J. Murata, M. Endo, T. Maeda, and Y. Kamada, “Experimental and numerical investigation of the effect of turbulent inflow on a Horizontal Axis Wind Turbine (part II: Wake characteristics),” Energy, vol. 113, pp. 1304–1315, Oct. 2016, doi: 10.1016/j.energy.2016.08.018.

[11] M. Talavera and F. Shu, “Experimental study of turbulence intensity influence on wind turbine performance and wake recovery in a low-speed wind tunnel,” Renew Energy, vol. 109, pp. 363–371, 2017, doi: 10.1016/j.renene.2017.03.034.

[12] K. Mikkelsen, “Effect of free stream turbulence on wind turbine performance.”

[13] Y. T. Wu and F. Porté-Agel, “Large-Eddy Simulation of Wind-Turbine Wakes: Evaluation of Turbine Parametrisations,” Boundary Layer Meteorol, vol. 138, no. 3, pp. 345–366, Mar. 2011, doi: 10.1007/s10546-010-9569-x.

[14] B. Panjwani, M. Popescu, J. Samseth, E. Meese, and J. Mahmoudi, “OffWindSolver: Wind farm design tool based on actuator line/actuator disk concept in OpenFoam architecture,” ITM Web of Conferences, vol. 2, p. 04001, 2014, doi: 10.1051/itmconf/20140204001.

[15] I. F. Syed Ahmed Kabir and E. Y. K. Ng, “Effect of different atmospheric boundary layers on the wake characteristics of NREL phase VI wind turbine,” Renew Energy, vol. 130, pp. 1185–1197, Jan. 2019, doi: 10.1016/j.renene.2018.08.083.

[16] P. J. Richards and S. E. Norris, “Appropriate boundary conditions for computational wind engineering models revisited,” Journal of Wind Engineering and Industrial Aerodynamics, vol. 99, no. 4, pp. 257–266, 2011, doi: 10.1016/j.jweia.2010.12.008.

[17] P. Å. Krogstad and J. A. Lund, “An experimental and numerical study of the performance of a model turbine,” Wind Energy, vol. 15, no. 3, pp. 443–457, 2012, doi: 10.1002/we.482.

[18] P. -Å. Krogstad and J. A. Lund, “An experimental and numerical study of theperformance of a model turbine - Krogestad”.

[19] M. Balogh and A. Parente, “Realistic boundary conditions for the simulation of atmospheric boundary layer flows using an improved k-ε model,” Journal of Wind Engineering and Industrial Aerodynamics, vol. 144, pp. 183–190, Sep. 2015, doi: 10.1016/j.jweia.2015.01.010.

[20] “ANSYS Fluent Theory Guide 15”.

[21] B. Blocken, T. Stathopoulos, J. Carmeliet, and B. Blocken, “CFD simulation of the atmospheric boundary layer: wall function problems,” 2007.

[22] J. Labovský and L. Jelemenský, “Verification of CFD pollution dispersion modelling based on experimental data,” J Loss Prev Process Ind, vol. 24, no. 2, pp. 166–177, Mar. 2011, doi: 10.1016/j.jlp.2010.12.005.

[23] D. Cabezón, E. Migoya, and A. Crespo, “Comparison of turbulence models for the computational fluid dynamics simulation of wind turbine wakes in the atmospheric boundary layer,” Wind Energy, vol. 14, no. 7, pp. 909–921, 2011, doi: 10.1002/we.516.

[24] D. C. Wilcox, Turbulence modeling for CFD. DCW Industries, 2006.

[25] Y. Yang, M. Gu, and X. Jin, “NEW INFLOW BOUNDARY CONDITIONS FOR MODELING THE NEUTRAL EQUILIBRIUM ATMOSPHERIC BOUNDARY LAYER IN SST k-ω MODEL.”

[26] Y. Yang, M. Gu, and X. Jin, “NEW INFLOW BOUNDARY CONDITIONS FOR MODELING THE NEUTRAL EQUILIBRIUM ATMOSPHERIC BOUNDARY LAYER IN SST k-ω MODEL.”

[27] R. Malki, I. Masters, A. Williams, and N. Croft, “Planning tidal stream turbine array layouts using a coupled blade element momentum - computational fluid dynamics model,” Renew Energy, vol. 63, pp. 46–54, Mar. 2014, doi: 10.1016/renene.2013.08.039.

[28] F. Russo and N. T. Basse, “Scaling of turbulence intensity for low-speed flow in smooth pipes,” Flow Measurement and Instrumentation, vol. 52, pp. 101–114, Dec. 2016, doi: 10.1016/j.flowmeasinst.2016.09.012.

[29] L. Li and R. J. Hearst, “The influence of freestream turbulence on the temporal pressure distribution and lift of an airfoil,” Journal of Wind Engineering and Industrial Aerodynamics, vol. 209, Feb. 2021, doi: 10.1016/j.jweia.2020.104456.